Article

Soil Moisture Retrievals Using Multi-Temporal Sentinel-1 Data over Nagqu Region of Tibetan Plateau

Mengying Yang, Hongquan Wang *, Cheng Tong, Luyao Zhu, Xiaodong Deng, Jinsong Deng and Ke Wang

College of Environmental and Resource Sciences, Zhejiang University, Hangzhou 310029, China;
21914160@zju.edu.cn (M.Y.); 21714124@zju.edu.cn (C.T.); luyao_zhu@zju.edu.cn (L.Z.); xddeng@zju.edu.cn (X.D.);
Jsong_deng@zju.edu.cn (J.D.); kwang@zju.edu.cn (K.W.)
* Correspondence: hongquan_wang@zju.edu.cn

Abstract: This paper presents an approach for retrieval of soil moisture in Nagqu region of Tibetan Plateau using VV-polarized Sentinel-1 SAR and MODIS optical data, by coupling the semi-empirical Oh-2004 model and the Water Cloud Model (WCM). The Oh model is first used to estimate the surface roughness parameter based on the hypothesis that the roughness is invariant among SAR acquisitions. Afterward, the vegetation water content (VWC) in the WCM is calculated from the daily MODIS NDVI data obtained by temporal interpolation. To improve the performance of the model, the parameters A, B, and α of the WCM are analyzed and optimized using randomly selected half of the sampled dataset. Then, the soil moisture is retrieved by minimizing a cost function between the simulated and measured backscattering coefficients. The comparison of the retrieved soil moisture with the ground measurements shows the determination coefficient R^2 and the Root Mean Square Error (RMSE) are 0.46 and 0.08 m^3/m^3, respectively. These results demonstrate the capability and reliability of Sentinel-1 SAR data for estimating the soil moisture over the Tibetan Plateau.

Keywords: Sentinel-1; MODIS; soil moisture; water cloud model; Oh model

1. Introduction

Soil moisture is an important variable in the earth ecosystem and a driving parameter for hydrologic, climate, and ecological models [1–4]. The spatial distribution and temporal evolution of soil moisture vary significantly [5,6], so it is of significance to study the spatiotemporal dynamic changes of soil moisture in a wide range. The traditional soil moisture information collected via the ground point measurements provides limited insight into the spatial distribution patterns of soil moisture at a short time interval.

With penetration capability through the vegetation canopy and atmospheric layers coupled with the advantage of all-weather observations [7], microwave remote sensing technology has achieved success in monitoring soil moisture over large-area [8]. Passive microwave remote sensing data on soil moisture retrieval has a long history and is relatively mature, but can be limited in terms of providing high-resolution detail. The synthetic aperture radar (SAR) in active microwave remote sensing has high spatial resolution and can capture the subtle spatial information features of the soil surface [9]. The Sentinel-1 mission composed of a constellation of two satellites provides high-resolution synthetic aperture radar (SAR) data. The double satellites increase their temporal resolution to six days [10]; thus, Sentinel-1 has received extensive attention in soil moisture retrieval [11]. Many studies have shown the appreciable capability of C-band Sentinel-1 SAR data in estimating soil moisture and vegetation parameters. For example, Vijay et al. [12] retrieved soil moisture through a modified water cloud model (WCM) and an improved inversion algorithm. Kumar et al. [9] estimated winter wheat crop growth parameters using time series of Sentinel-1A SAR data.

The SAR backscattering coefficient is sensitive to soil dielectric constant, which is directly related to soil moisture content, laying a solid physical foundation for microwave

remote sensing retrieval of soil moisture [13]. However, in addition to being controlled by soil dielectric properties, the backscattered signal is strongly influenced by vegetation and surface roughness [14]. The quantification of the respective contributions from vegetation and surface roughness affects the accuracy of soil moisture retrieval. Nevertheless, the interaction between ground object and radar scattering signal is complex, and the scattering mechanisms are sophisticated due to the overlaps among surface, volume, and dihedral scatterings. This leads to relatively large uncertainty in the subsequent soil moisture retrieval [15,16]. The developments of the soil moisture retrieval methods based on SAR observation have been a hotspot and difficult area.

Vegetation scattering models describe the microwave scattering process within the vegetation canopy. So the coupling of the vegetation scattering model and bare soil scattering model may eliminate the influence of surface roughness and vegetation cover to improve the accuracy of retrieval. For bare soil, scattering models mainly include empirical/semi-empirical models, such as the Oh-2004 model [17] and Dubois model [18], and theoretical models such as the Integral equation model (IEM) and the Advanced IEM (AIEM) [19–21]. These models were evaluated on the TerraSAR-X data over the bare soils, and the Oh model provided the best results [22]. The Oh-2004 model simulates the radar backscattering coefficient in term of soil moisture to avoid the intermediate processing of converting the dielectric constant from soil moisture. In this model, only the root mean square height (RMSH) was used to characterize the surface roughness, which reduces the number of unknown parameters and the uncertainty in the inversion process. Compared to theoretical models such as IEM and AIEM, this model has a simple formula and a higher efficiency in retrieval process. For vegetation cover areas, the commonly used scattering models mainly include the WCM [21] and the MIMICS model [23]. The WCM supposes the backscattering coefficient is composed of the contributions from the vegetation canopy and soil surface. The MIMICS takes into account additional backscattering components, such as plant–ground and ground–plant interactions, as well as ground–plant–ground scattering contributions. However, for the low grass condition over the Tibetan Plateau, the WCM with a smaller number of unknown parameters is more suitable to retrieve the soil moisture than the MIMICS [22,24–26]. Consequently, the WCM and Oh models are often coupled to estimate soil moisture in the vegetated area. The WCM describes the vegetation characteristics using the Vegetation Water Content (VWC) which can be estimated from optical remote sensing data [27].

In [26], different radiative transfer models were evaluated over the wheat fields using the Sentinel-1 data. The LAI along with the dynamic empirical parameters seems better to capture the variation of the backscattering coefficients than the static empirical parameters. Furthermore, the WCM was calibrated using C-band Sentinel-1 data over the agricultural and grass lands. The NDVI extracted from the Sentinel-2 optical data was used as a vegetation descriptor in the WCM, and the IEM was applied to interpret the surface scattering component. Based on the radiative transfer models, a variety of SAR soil moisture retrieval algorithms were formed, such as change detection, optimization cost function, linear/nonlinear interpolation, lookup table, Bayesian posterior estimation, and artificial neural network [28]. The change detection was used to monitor surface soil moisture over the heterogeneous areas [29]. The cost function algorithm was optimized to estimate soil moisture [30,31]. The statistical relationships between radar backscattering coefficient and surface soil moisture were approximated as linear [32], exponential [33], or polynomial [34]. The process of lookup table retrieval is similar to that of least squares interpolation retrieval [35,36]. The Bayesian posterior estimation and artificial neural network were also evaluated to retrieve the soil moisture from remote sensing data [37]. Among them, the cost function optimization method which estimates the surface parameters by iteratively minimizing system errors, is considered with high universality and reliability [38,39]. The optimal estimates are constrained by physical significance and global optimization status [10,40].

Considered as the "Third Pole of the Earth", the Tibetan Plateau is the highest one in the world. Soil moisture is one of the most sensitive factors affecting precipitation patterns and water cycles in this region due to its unique topographical features, so an adequate understanding of the soil moisture over the Tibetan Plateau is necessary. Considerable pioneer soil moisture retrieval works have been done over the Tibetan Plateau, either through radiometer [41], or radar signals [42]. However, it is still necessary to evaluate the impact of different vegetation and soil parameterization on the accuracy of soil moisture retrievals. Compared to [42] which used AIEM for surface component and LAI for characterization of the vegetation, we used the Oh model for surface component and applied an empirical relationship between the VWC and NDVI. The purpose of our study is to analyze the potential of the combination between Sentinel-1 SAR and MODIS imageries for soil moisture retrieval on the Tibetan Plateau. We couple the Oh-2004 [17] model into the WCM [15,43] to simulate SAR backscatter, then construct a cost function to minimize the difference between the model simulated and Sentinel-1 observed backscatters and to search for the optimal solution for soil moisture retrieval.

The novelty of this paper relies in the following aspects: (1) We utilized a modified volume scattering component σ_{veg}^0 in which a radar-shadow coefficient is introduced for the WCM model. (2) The Sentinel-1 SAR data were combined with MODIS imageries to retrieve soil moisture over the Tibetan Plateau. Since the soil moisture is one of the most sensitive factors affecting precipitation patterns and water cycles in this region, an adequate understanding of the soil moisture is necessary considering the unique topographical features. (3) A transfer function between VWC and NDVI [44] was evaluated to estimate the VWC for the study area. This may benefit the selection of transfer function to obtain the VWC parameter which is essential to parameterize the radar backscattering coefficient. Therefore, the current study deepens the understanding on the optical–microwave jointing estimation of soil moisture over the Tibetan Plateau. The outline of this paper was given as follows: Section 2 presents the details of the study area, in situ moisture, and Sentinel-1 SAR and Terra MODIS data. Section 3 describes the details of methodology, including vegetation and soil backscatter decomposition, model calibration, and soil moisture retrieval, followed by Section 4 for result analysis. Section 5 discusses the potential uncertainty in soil moisture retrieval, followed by the conclusions in Section 6.

2. Study Site and Datasets

2.1. Study Site

The study site is located in Nagqu, northern Tibet, in the hinterland of the Tibetan Plateau (Figure 1). Nagqu plays a key role in terrestrial energy balance. The selected site has an average altitude of above 4500 m. Despite this altitude, the terrain is relatively flat, with rolling hills varying only a few dozen meters in elevation. The vegetation cover is mainly high-situated pasture. Its climate is characterized by extreme cold and hypoxia, dry and windy. The annual average temperature is −0.9 °C to −3.3 °C, the annual relative humidity is 48–51% and the annual precipitation is 380 mm [45]. From November to the following year in March, it is a dry and windy period. From April to October, the climate is relatively warm, and it is the golden growing season of grassland. For this mountainous area, the soil moisture dynamics have a large spatial variability [46]. Therefore, this area is selected for our study to develop and validate a soil moisture retrieval algorithm using the Sentinel-1 and MODIS data.
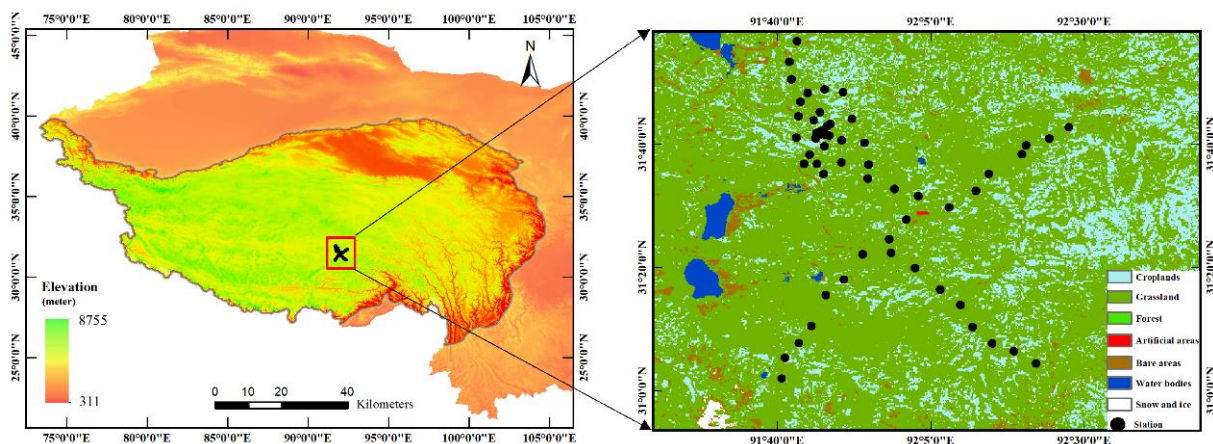
Figure 1. Location of soil moisture stations over Tibetan Plateau.

2.2. In Situ Soil Moisture

The in situ soil moisture data are obtained from the Nagqu soil moisture and temperature network in the central Tibetan Plateau. The network contains 56 soil moisture stations (Figure 1). This network (ISMN: https://ismn.geo.tuwien.ac.at/en/) provides soil moisture and temperature with a time interval of 30 min at four different depths (0~5 cm, 10 cm, 20 cm, and 40 cm) from 2011 to 2016 [47,48]. The details of the Nagqu network can be found in Yang et al. [49]. Considering the potential penetration depth at C-band, this study selects the in situ soil moisture measurements at the top soil layer (0~5 cm) for the model evaluation and validation. However, there is a serious data loss, as part of the Sentinel-1 images can not completely cover the 56 stations. By appropriate screening, 43 stations are selected for further research. In addition, we have made quality control of the in situ soil moisture data according to ISMN Quality Flags. Figure 2 shows the temporal evolution of the mean values of the measured soil moisture and temperature over the 43 stations from April to November 2015, which indicate a seasonal variability.
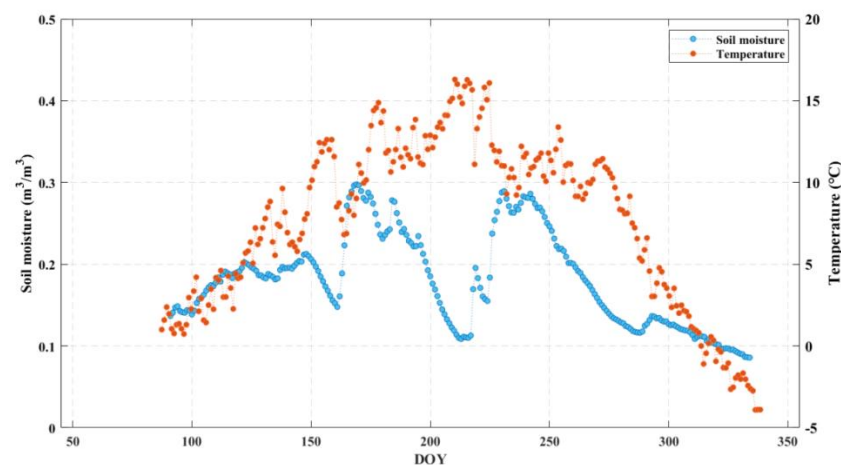

Figure 2. Temporal profile of averaged soil moisture and temperature measured over the 43 stations in 2015.

2.3. Sentinel-1 SAR Data

Sentinel-1 is the European Space Agency's (ESA) Copernicus Earth Observation satellite. It consists of two satellites carrying C-band synthetic aperture radar with a central frequency of 5.405 GHz. Since the revisit period of a single satellite is 12 days, and that of A/B twin satellites reduces to 6 days. The SAR has a variety of imaging modes: Striped Map (SM), Interferometric Wide Swath (IW), and Extra Wide Swath (EM). We adopt the Ground

Range Detected (GRD) product of IW mode with VV and VH dual-polarized modes and spatial resolution 5 m × 20 m. Many studies have shown that the cross-polarized VH channel is more sensitive to vegetation change, while co-polarized VV is sensitive to both vegetation and soil moisture, and thus the latter has greater potential in soil moisture retrieval [50,51]. Therefore, only VV polarized backscatter signal is selected in this study.

The Sentinel-1 Level 1 products including 38 scenes from April to November 2015, were downloaded from the Sentinel Data Hub website (https://scihub.copernicus.eu/). The full preprocessing chain comprises: (1) radiometric calibration to reduce radiation deviation; (2) refined Lee speckle filter with 5 × 5 windows to reduce the speckle noise; and (3) geometric corrections (Range-Doppler terrain correction) to correct the distortion of ground objects in radar images with 30 m SRTM DEM. The preprocessing is conducted using the SNAP software.

Given the spatial heterogeneity of soil moisture, buffer zones with a 200 m radius are established for each of the 43 ground stations in the study area. Then, the backscattering coefficients at VV polarized and the associated local incidence angle of each station are extracted and averaged for the model development.

2.4. MODIS Data

MODIS has two sensors that operate on the Terra and Aqua spacecraft, respectively. Both the Terra NDVI (MOD13Q1) and Aqua NDVI (MYD13Q1) are level-3 grid data in the Sinusoidal projection mode at 250 m spatial resolution and the 16-day temporal resolution derived from daily surface reflectance by selecting the high-quality pixels (https://search.earthdata.nasa.gov/search) [52]. Since the Terra NDVI data are used to characterize the vegetation dynamics in the current study, we perform a temporal interpolation on the Terra NDVI products in order to match them to the Sentinel-1 data acquisition time. Before the analysis, the two datasets need to be preprocessed via the MODIS Re-Projection Tool (MRT), including re-projection, file format conversion and spatial composition. Then the NDVI data for the soil moisture stations are extracted using the same buffer established for the Sentinel-1 SAR data. To verify the accuracy of the interpolation result, the daily mean NDVI derived from the interpolation of Terra NDVI data are compared with Aqua NDVI data in the corresponding period. Figure 3 shows a high consistency between the interpolated NDVI values and the Aqua NDVI products over a representative station L02. The study area is covered by grass, and the temporal variation of the interpolated NDVI can well capture the phenological rhythms of the grass growths (Figure 3). Consequently, the NDVI dataset obtained by interpolation will be used to describe the vegetation influences on the radar backscattering coefficient.
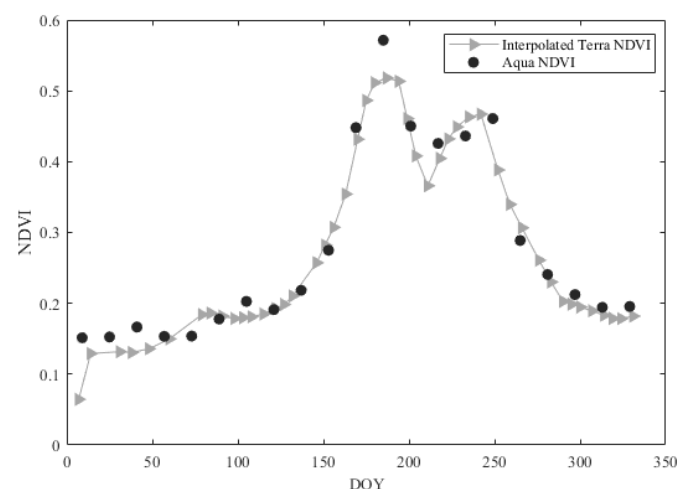

Figure 3. Comparison of interpolated Terra NDVI with Aqua NDVI products over a representative station (L02) in 2015.

3. Methodology

In this paper, the Oh-2004 model and the WCM are coupled to simulate the backscattering coefficients at VV polarization for Sentinel-1 SAR data. MODIS data are used to compute the vegetation contribution in the SAR backscattering coefficients. By optimizing a cost function constructed by the model simulations and SAR observations, the soil moisture was retrieved. The implementation of the coupled model calibration and soil moisture retrieval is illustrated in Figure 4, and detailed development of the coupled model is described in the following sections.
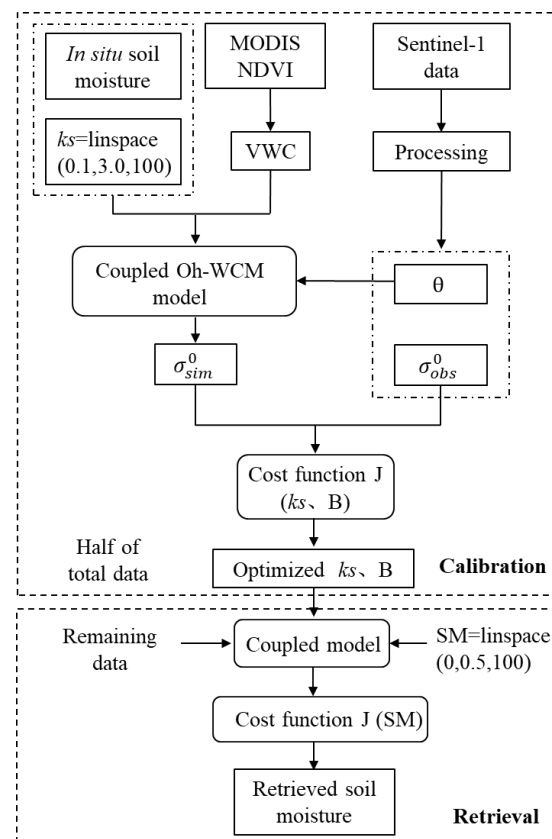

Figure 4. Diagram of model calibration and retrieval of soil moisture.

3.1. Vegetation and Soil Backscatter Decomposition

Since the vegetation disturbance is an important factor affecting the accuracy of soil moisture retrieval, we apply the WCM to correct the vegetation effect. This model is an empirical model proposed by Attema and Ulaby for agricultural crops, and has a wide range of applications [43]. The model makes the following hypothesis: (1) the vegetation is represented as a homogeneous horizontal cloud of identical water spheres, uniformly distributed throughout the space defined by the soil surface and the vegetation height. (2) the double bounce power is relatively low due to the shallower penetration depth at C-band, so it is theoretically appropriate to ignore the double-bounce component. According to [53], the dihedral scattering power at C-band is less than 10% during the entire phenological stages. In [54], the dihedral scattering power was also found low at C-band, and can be neglected in the WCM. Therefore, the total backscatter signal received by radar can be expressed as:

$$\sigma^0_{total} = \sigma^0_{veg} + \tau^2 \sigma^0_{soil} \tag{1}$$

where σ^0_{total} is the total SAR backscattering coefficient, σ^0_{veg} and σ^0_{soil} are the backscatters from vegetation and underlying soil, respectively.

3.1.1. Surface Component

The backscattering from the bare soil surface is simulated by the semi-empirical Oh-2004 model. In this model, the surface roughness is described using surface Root Mean Square height (RMSH), without considering the autocorrelation length. From the aspect of soil moisture retrieval, reducing the number of unknowns reduces the uncertainty of the retrieval [55]. Consequently, the *VV*-polarized backscattering coefficient of the bare soil surface can be expressed as:

$$\sigma_{VV}^{0} = \frac{0.11 SM^{0.7} [\cos(\theta)]^{2.2} \left[1 - e^{-0.32(ks)^{1.8}}\right]}{0.095[0.13 + \sin(1.5\theta)]^{1.4} \left[1 - e^{-1.3(ks)^{0.9}}\right]} \tag{2}$$

where *SM* is the soil moisture; θ is incidence angle; *k* and *s* are the wavenumber and RMSH (cm), respectively. The validity of Oh model was tested for $0.04 < SM < 0.29 \text{ m}^3/\text{m}^3$, $0.13 < ks < 6.98$ and $10° < \theta < 70°$ [25,26].

3.1.2. Volume Component

In a radar beam, two or more canopies usually overlapped, leading to overestimation of the vegetation backscatter due to the canopy layover and radar shallow. Thus, we utilize a modified volume scattering component σ_{veg}^{0} in which a radar-shadow coefficient is introduced to account for the effect of vegetation layover [15]:

$$\sigma_{veg}^{0} = A \text{ VWC } \cos(\theta) \left(1 - \tau^2\right) \left(1 - e^{-\alpha}\right) \tag{3}$$

$$\tau^2 = e^{-2B \text{ VWC}/\cos(\theta)} \tag{4}$$

where θ is the incidence angle, VWC (kg/m^2) is the vegetation water content as computed by NDVI; τ^2 is the two-way vegetation transmissivity, which can be obtained by parameterization of VWC. A and B are the empirical parameters of the model depending on the canopy type, α is the radar-shadow coefficient depending on vegetation type and land use.

The NDVI was used to estimate the VWC, which comprised of the foliage water content derived from the NDVI, and the stem water content derived from annual NDVI extremes along with a coefficient of stem factor [44]:

$$\text{VWC} = \left(1.9134 \times \text{NVDI}^2 - 0.3215 \times \text{NVDI}\right) + stem\ factor \times \frac{\text{NVDI}_{max} - \text{NVDI}_{min}}{1 - \text{NVDI}_{min}} \tag{5}$$

where the NDVI is obtained from the MODIS-Terra MOD13Q1 product, NDVI_{max} and NDVI_{min} represent the annual maximum and minimum values of the NDVI for a given location. The stem factor as a product of average vegetation height and the ratio of sapwood area to leaf area, represents an estimate of the peak amount of water residing in the stems, and depends on vegetation types. The default value of stem factor is set at 1.5 when the vegetation type is grassland [56]. However, considering the low grass covering the study area, this default value may be too high. Therefore, in this study, we adjusted the factor to 0.3 [57]. By adjusting the stem factor, the Equation (5) match well to the ground measurements, and maintain the reasonable temporal behavior of VWC in term of vegetation growth phenology.

3.2. Model Calibration and Soil Moisture Retrieval

The parameters (A, B and α) in Equation (3) were determined based on randomly selected 50% of the data. The remaining 50% data were used to retrieve the soil moisture, followed by the validation against the ground measurements. To obtain globally optimal

solutions for different parameters, we minimized a cost function J (dB) was constructed using the simulated backscattering coefficients (σ_{sim}^0) and radar observations (σ_{obs}^0):

$$J = \sqrt{\frac{1}{n} \sum \left(\sigma_{obs}^0 - \sigma_{sim}^0\right)^2} \qquad (6)$$

3.2.1. Surface Roughness

The surface roughness was regarded stable over a short time [30], and optimized using Oh-2004 model applied to the SAR data acquired under bare and unfrozen soil conditions. We choose the Sentinel-1 image and the ground measured soil moisture collected on 1 April 2015 for which the soils are not covered by vegetation as input data to estimate the roughness [31]. In the process, roughness *ks* is set as a free parameter ranging between 0.1 and 3.0 to iteratively match the model simulations to the Sentinel-1 SAR backscattering coefficient.

3.2.2. Parameters A, B and α

To examine the influence of the parameters A, B and α of the WCM on soil moisture retrieval, we conducted a synthetic simulation experiment to observe the sensitivity of the SAR backscattering coefficient to the variations of the involved vegetation parameters. The experiment consists of three individual tests. For each test, only one parameter varies within its range, the other two parameters are fixed. The ranges of the parameters variation are set according to Table 1 from the findings in Bindlish and Barros [15]. In all three tests, the value of VWC ranges from 0 to 1.0 with an interval of 0.2 kg/m^2. Based on the simulation, the cost function is used again to calibrate the parameters.

Table 1. Values of vegetation parameters used in the semi-empirical model.

	All Land-Uses	Rangeland	Winter Wheat	Pasture
A	0.0012	0.0009	0.0018	0.0014
B	0.091	0.032	0.138	0.084
α	2.12	1.87	10.6	1.29

3.2.3. Retrieval of Soil Moisture

In the retrieval process, the calibrated parameters A, B and α and the estimated surface roughness are brought into Equation (6), and the soil moisture is set as a free parameter to iteratively match the simulated backscattering coefficients to the Sentinel-1 SAR observations. Finally, the retrieved soil moisture is validated against the ground measurements.

4. Results

This section analyzes the estimated surface roughness, parameters of the WCM and soil moisture by applying the proposed approach to the Sentinel-1 SAR and MODIS data.

4.1. Sensitivity of Sentinel-1 Backscatters to Surface Parameters

To explore the response of SAR backscattering coefficients to the variations of soil moisture and NDVI, a simple regression analysis is first conducted. As shown in Figure 5, there is a relatively weak positive correlation between the backscattering coefficient and soil moisture (Figure 5a). The deviation of the points from the fitted line is attributed to the differences in vegetation condition, surface roughness and local incidence angle at different stations. A similar weak sensitivity of the C-band SAR backscattering coefficient to measured soil moisture is observed in many previous studies due to the joint effects of soil and vegetation parameters [29,32,58]. In Figure 5b, the influence of the vegetation on the backscattering power was observed. In addition, with an increasing NDVI, an increasing trend is observed in soil moisture (Figure 5c), confirming close coupling between vegetation

and soil moisture. Thus, in order to retrieve soil moisture from C-band Sentinel-1 SAR data, it is necessary to better parameterize the vegetation contribution.
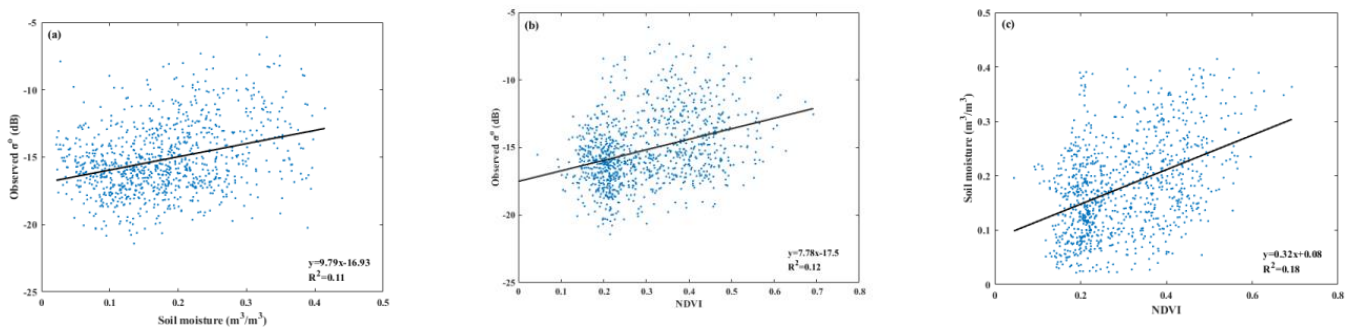

Figure 5. Sensitivity of SAR backscattering coefficients to (**a**) ground measured soil moisture, (**b**) NDVI, and (**c**) relationship between ground measured soil moisture and MODIS NDVI.

4.2. Estimated Surface Roughness

In this process, we applied Equation (2) to the VV polarized backscattering and ground measurements, resulting in surface roughness values for 43 soil moisture ground stations (Figure 6a). In addition, the mean soil temperature (Figure 6b) and NDVI (Figure 6c) were verified to ensure unfrozen and bare soil moisture on 1 April 2015. Most values of the surface roughness *ks* range from 0.3 to 0.7. Previous studies have estimated the surface roughness parameters of these stations [31], and s is mostly distributed between 0.2 and 0.6, demonstrating that the values of *ks* are consistent with our estimated results.
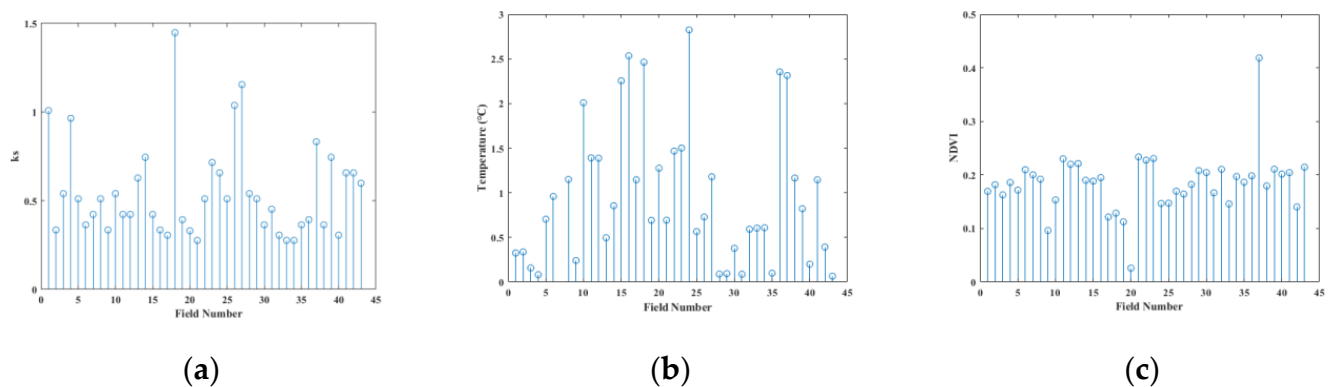

(a)   **(b)**   **(c)**

Figure 6. (**a**) Optimized surface roughness, (**b**) Ground measured soil temperature (no temperature data for L07-M13 station), and (**c**) NDVI for 43 ground stations on 1 April 2015.

Based on the optimized surface roughness parameters and the measured soil moisture, the backscattering coefficient is simulated. In Figure 7, a relatively high correlation between the simulated backscattering and Sentinel-1 SAR data at VV polarized channel was found. It indicates the feasibility of optimizing the assumed stable surface roughness parameters prior to retrieving the soil moisture.
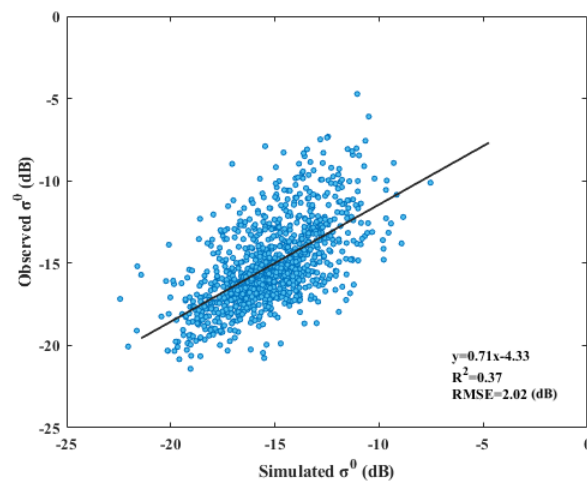
Figure 7. Comparison between measured and simulated SAR backscattering coefficients using the optimized surface RMSH.

4.3. Optimized Vegetation Parameters A, B, and α

Before the optimization, the sensitivity of simulated SAR backscattering coefficients to the variation of the vegetation parameters (A, B, and α) is analyzed for six different VWC levels. Figure 8 shows the response of simulated backscatters to the three vegetation parameters. As can be seen in Figure 8a,c, almost no changes are observed with increasing values of parameters A and α, but with different VWC levels, the backscatters show a certain difference. In contrast, in Figure 8b, the backscattering coefficients decrease with increasing values of parameter B and the variation amplitude increases with the increase of VWC. It indicates that parameters A and α are not sensitive to soil moisture retrieval, so parameter B should be mainly calibrated in the subsequent process. Similar observations for the vegetation parameters were found in previous studies [59]. Thus, the values of parameters A and α, are set to the "all land uses" values in Table 1. In Figure 9, the parameter B iterates between 0.03 to 0.14 with 100 intervals, and the lowest J value was obtained when B is equal to 0.05.
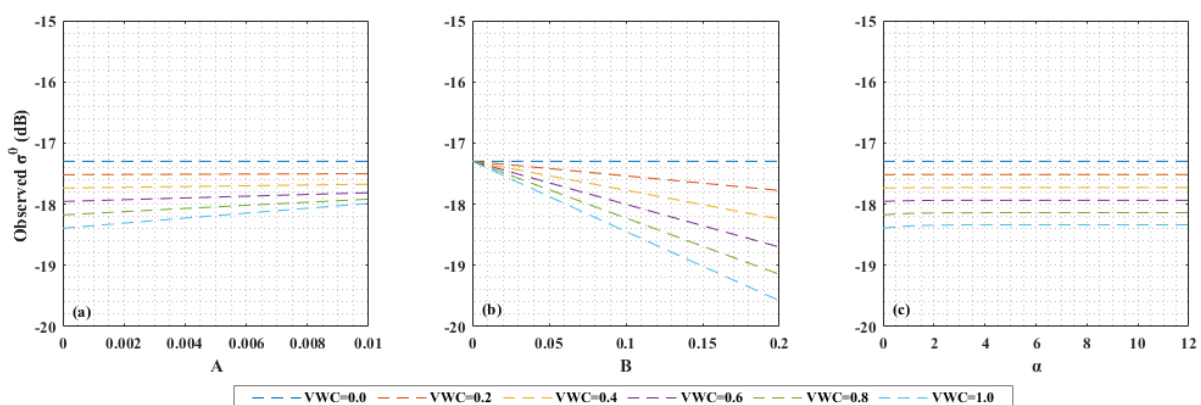

Figure 8. Response of SAR backscatters to variation of vegetation parameters (**a**) A, (**b**) B, and (**c**) α in WCM.
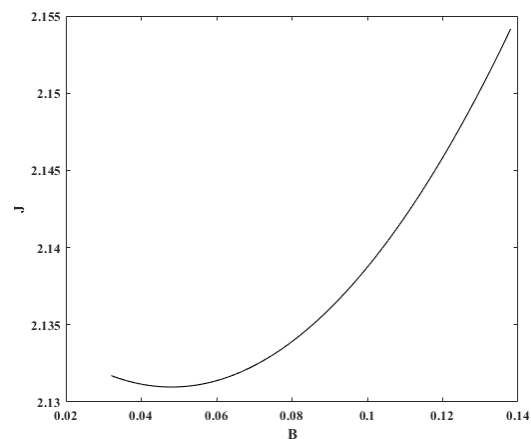
Figure 9. The values of function J under different settings of parameter B.

4.4. Retrieved Soil Moisture

After the calibration of the coupled Oh-2004 and WCM model, the remaining 50% Sentinel-1 data are used for soil moisture retrieval. As shown in Figure 10, the retrieved soil moisture shows consistency with observations over the ground stations. However, two outliers circled in red are found, with a large overestimation. The NDVI values for the two outliers are 0.25 and 0.33, which are lower than the averaged 0.53 for all the stations. On the other hand, their respective ks values are 1.0 and 0.96, which are significantly higher than the averaged 0.3 for all the stations, but still in the validity range of the Oh model. Nevertheless, the combined effects of higher roughness and lower vegetation condition result in a similar level of radar backscattering coefficient as the mean value across all the stations. Except for these two outliers, a determination correlation $R^2 = 0.46$ and root-mean-square error RMSE = 0.08 m^3/m^3 were obtained. This indicated that the combination between Sentinel-1 SAR and MODIS optical remote sensing data is feasible to retrieve soil moisture over the Tibetan plateau.
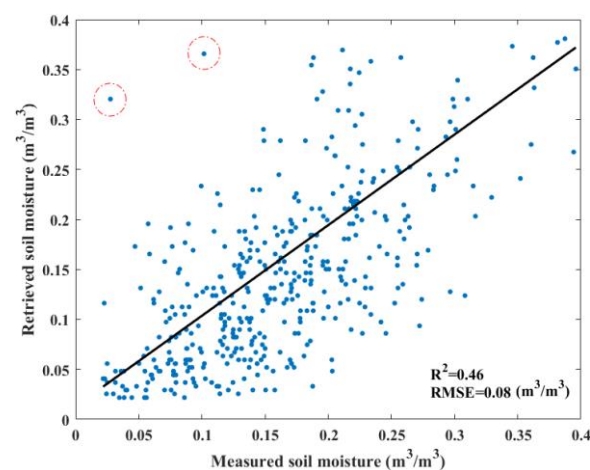

Figure 10. Scatterplots between measured and retrieved soil moisture for all stations.

Furthermore, Figure 11 shows the temporal profiles of the retrieved and measured soil moisture over four stations for a more detailed analysis. To a certain extent that the soil moisture is closely related to the MODIS NDVI. This result is consistent with our previous sensitivity analysis (Figure 5). The more water exists in the soil, the more vegetation grows which increases MODIS NDVI values. Vegetation growth and enhanced density also help to maintain the water particles in the soil layer. This indicates that the interaction between soil moisture and NDVI is a bidirectional process. The temporal variation of trends of

the retrieved soil moisture is consistent with the ground measurement. However, the deviation was observed over station M05 probably due to the variation of topography. Over the station M05, the incidence angle is above 50°, higher than the average value 38.6° across all the stations. As the incidence angle increases, the vegetation contribution dominates the backscattering power, while the soil contribution decreases leading thus to an underestimation of soil moisture.
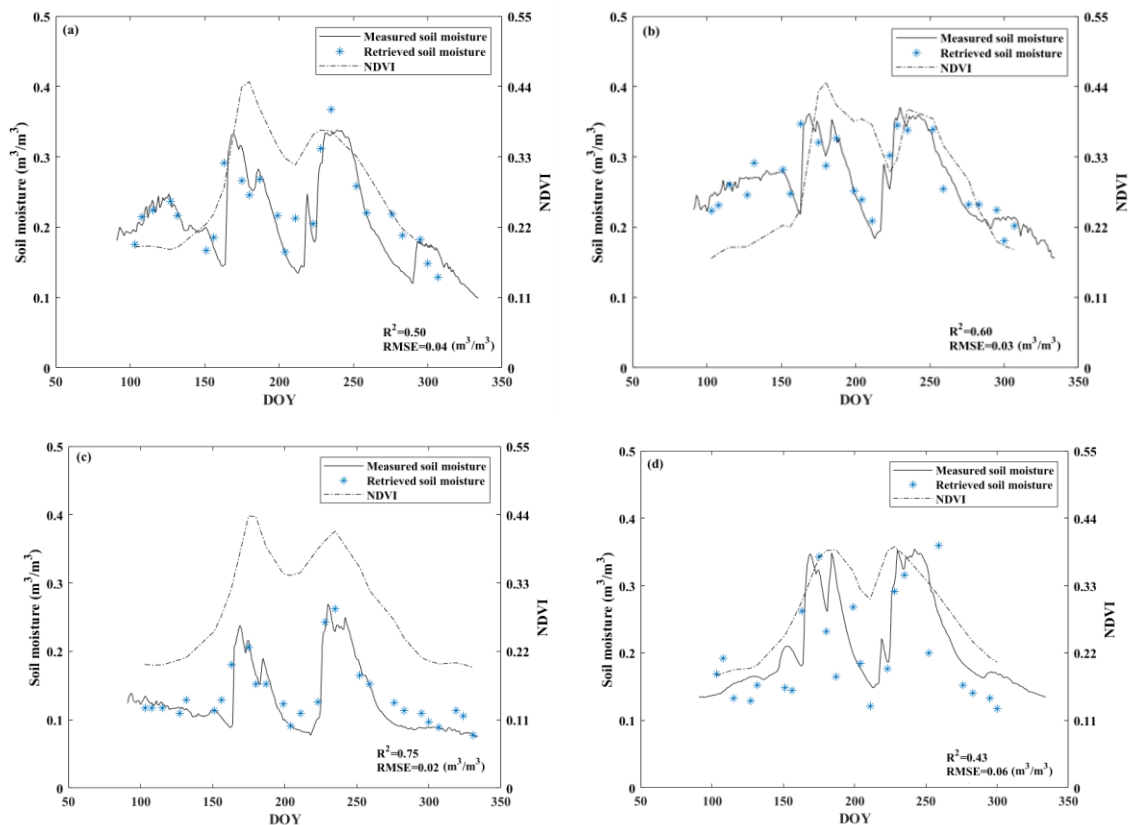

Figure 11. Time series of measured and retrieved soil moisture, with respect to NDVI over four stations (**a**) L04-M02, (**b**) L05-M06, (**c**) L07-M13, (**d**) M05.

5. Discussion

In our study, the Oh-2004 and the WCM are coupled to estimate the soil moisture from VV-polarized Sentinel-1 SAR and MODIS data in Nagqu. We propose to decompose the backscattering coefficients into vegetation canopy volume scattering and soil surface scattering mechanisms, and obtain soil moisture from the latter soil-related components. As can be seen from the retrieval results with a determination coefficient $R^2 = 0.46$ and the RMSE $= 0.08$ m^3/m^3, this accuracy is within a similar level as the literature. For instance, Bai et al. [42] estimated soil moisture over Tibetan Plateau by coupling the WCM and the AIEM. The retrieval results are with R^2 equal to 0.36 and 0.67, and RMSE of 0.073 m^3/m^3 and 0.055 m^3/m^3 for the ascending and descending data, respectively. Compared to [60] which applied the IEM model to multi-angular ASAR data over Tibetan Plateau, our method with the vegetation correction obtain better results. Chai et al. [61] used RADARSAT-2 imagery to model and map soil moisture of Plateau Pasture, with R^2 ranged from 0.59 to 0.7 and RMSE ranged from 0.043 to 0.048 m^3/m^3.

Nevertheless, the performance of the approach is subject to incident angle, vegetation and surface roughness parameters. The radar incidence angle determines the direction and transmission path of the radar beam. With the increase of incident angle, the distance of microwave propagation, and the amount of vegetation penetrated gradually increased [62]. Therefore, the soil contribution decreases while vegetation contribution predominates at a

high incidence angle. There is an approximately exponential dependence between surface roughness and backscattering coefficient, and this dependence is more significant with the increase of incident angle [63]. Thus, the high incident angle makes it challenging to monitor soil moisture. This phenomenon was confirmed over the station M05 where an underestimation of soil moisture was found due to the high incidence angle.

The performance is also affected by assumptions made for the development of the algorithm. In our current study, the surface roughness which is derived by hypothetical bare and unfrozen soil conditions is assumed to be temporally stable during the Sentinel-1 acquisitions. However, the roughness parameter may be modified by rainfall or human factors [64]. Previous researches have indicated that stable roughness parameters are unable to characterize the changeability of the soil surface [65]. It is better to update the effective roughness parameters for each acquisition. In our case with a single polarization radar configuration, the elimination of the roughness effect is challenging, since the roughness significantly varies with local incidence angle, microwave frequency and polarization. Thus, multi-dimensional SAR configurations are necessary to refine the parameterization of the soil surface roughness on the soil moisture retrievals [66,67]. Furthermore, in the equation system, the estimation accuracy of effective roughness parameters has an important impact on the calibration of the WCM parameters A, B, and α, and thus affect the subsequent retrieval of soil moisture.

In addition to the impact of surface roughness, parameters A, B, and α in the WCM also have an impact on soil moisture retrieval. Since the coefficients of the WCM model are empirically fitted, the representability of the training data impacts the performance of the model. For test sites with different vegetation characteristics, the empirical coefficients need to be tuned. In our study, to reduce the number of known parameters, we first carried out a simulation analysis, and concluded that the VV-polarized backscattering coefficient had the highest sensitivity to the change of parameter B compared to the two other parameters. Based on this conclusion, the subsequent calibration was focused on parameter B, while A and α are directly taken from the previous studies. Furthermore, the Vegetation Water Content was derived from the NDVI. Nevertheless, with the increase of NDVI value, the sensitivity of radar signal to soil moisture decreased, increasing the uncertainty in extracting the soil moisture information [68]. In the following work, it is necessary to refine the parameterization of vegetation parameters in the WCM by extensive vegetation ground measurements.

Furthermore, in our current experiment, we randomly selected the training data to calibrate the parameters in WCM, which were then used in the further retrieval of soil moisture. We repeated the test for 10 times and found that the calibration with different training datasets may result in slightly different values of calibrating parameters. Although the results of soil moisture retrieval are affected by the selection of training datasets, this effect is relatively small over the same study area. The uncertainty caused by selecting different datasets is partially compensated by the associated parameter calibration.

Finally, the optimization algorithm used in the calibration step impacts the accuracy of soil moisture retrieval. Although we used a cost function to determine the vegetation parameters in WCM, other sophisticating optimization approaches such as the genetic algorithm may be considered as alternative approaches. In addition, the iterative loop setting and the convergence conditions also influence the optimization of the WCM parameters and the accuracy of subsequent soil moisture retrieval. In the current paper, as the number of iterations reaches around 100, the RMSE of the retrieval result tends to converge stably and the calculation time is relatively small.

6. Conclusions

In this paper, we combined the Oh-2004 model with the WCM to conduct soil moisture retrieval in Nagqu region of Tibetan Plateau using the sentinel-1 SAR and MODIS optical data. The main conclusions are summarized as follows:

We carry out a linear interpolation on the MODIS NDVI 16-days composites to obtain the daily NDVI, then substitute it into an empirical model (Equation (5)) to calculate the corresponding vegetation water content. The result demonstrates the temporal interpolation for limited measured vegetation growth parameters is feasible to capture the vegetation dynamics. The retrieved and measured soil moisture were close related to the NDVI, indicating the coupling mechanism of the soil–vegetation system.

As for roughness, we assume that it is stable over a relatively short time, and estimate it by inverting the backscattering coefficient of a SAR image acquired at bare soil conditions. Since the land cover in the study area is mainly grassland, and the variation of land surface attributes is small. Therefore, this assumption is reasonable to reduce the surface roughness effect on soil moisture retrieval.

The observed inconsistencies between the in situ measurement and retrieved soil moisture mainly attribute to the representativity of model calibration and the quality of vegetation parameters. Additional investigation of these factors is likely to provide a deeper insight into soil moisture retrieval. Although the Sentinel-1 SAR-based soil moisture retrieval remains challenging, the precise scale of SAR data is significantly important for agricultural and water management applications, as well as for the further development of land surface and hydrologic process models.

References

1. Jackson, T.J., III. Measuring surface soil moisture using passive microwave remote sensing. *Hydrol. Process.* **2010**, *7*, 139–152. [CrossRef]
2. Seneviratne, S.I.; Corti, T.; Davin, E.L.; Hirschi, M.; Jaeger, E.B.; Lehner, I.; Orlowsky, B.; Teuling, A.J. Investigating soil moisture–climate interactions in a changing climate: A review. *Earth Sci. Rev.* **2010**, *99*, 125–161. [CrossRef]
3. Scipal, K.; Drusch, A.; Wagner, W. Assimilation of a ERS scatterometer derived soil moisture index in the ECMWF numerical weather prediction system. *Adv. Water Resour.* **2008**, *31*, 1101–1112. [CrossRef]
4. Pangaluru, K.; Velicogna, I.; Geruo, A.; Mohajerani, Y.; Ciracì, E.; Cpepa, S.; Basha, G.; Rao, S. Soil moisture variability in India: Relationship with land-surface atmospheric fields using Maximum Covariance Analysis. *Remote Sens.* **2019**, *11*, 335. [CrossRef]
5. Jin, R.; Li, X.; Liu, S.M. Understanding the Heterogeneity of Soil Moisture and Evapotranspiration Using Multiscale Observations From Satellites, Airborne Sensors, and a Ground-Based Observation Matrix. *IEEE Geosci. Remote Sens. Lett.* **2017**, *14*, 2132–2136. [CrossRef]
6. Li, X. Characterization, controlling, and reduction of uncertainties in the modeling and observation of land-surface systems. *Sci. China Earth Sci.* **2014**, *57*, 80–87. [CrossRef]
7. Ulaby, F.T.; Moore, R.K.; Fung, A.K. *Microwave Remote Sensing: Active and Passive. From Theory to Application*; Artech House: Norwood, MA, USA, 1986.
8. Kumar, S.T.; Bitar, A.A.; Sekhar, M.; Zribi, M.; Bandyopadhyay, S.; Kerr, Y. MAPSM: A Spatio-Temporal Algorithm for Merging Soil Moisture from Active and Passive Microwave Remote Sensing. *Remote Sens.* **2016**, *8*, 990. [CrossRef]

9. Kumar, P.; Prasad, R.; Gupta, D.K.; Mishra, V.N.; Vishwakarma, A.K.; Yadav, V.P.; Bala, R.; Choudhary, A.; Avtar, R. Estimation of winter wheat crop growth parameters using time series Sentinel-1A SAR data. *Geocarto Int.* **2017**, *33*, 1–24. [CrossRef]

10. Paloscia, S.; Pettinato, S.; Santi, E.; Notarnicola, C.; Pasolli, L.; Reppucci, A. Soil moisture mapping using Sentinel-1 images: Algorithm and preliminary validation. *Remote Sens. Environ.* **2013**, *134*, 234–248. [CrossRef]

11. Potin, P.; Rosich, B.; Miranda, N.; Grimont, P.; Shurmer, I.; O'Connell, A.; Krassenburg, M.; Gratadour, J.B. Copernicus Sentinel-1 Constellation Mission Operations Status. In Proceedings of the International Geoscience and Remote Sensing Symposium, Yokohama, Japan, 28 July–2 August 2019.

12. Yadav, V.P.; Prasad, R.; Bala, R.; Vishwakarma, A.K. An improved inversion algorithm for spatio-temporal retrieval of soil moisture through modified water cloud model using C- band Sentinel-1A SAR data. *Comput. Electron. Agric.* **2020**, *173*, 105447. [CrossRef]

13. Dobson, M.C.; Ulaby, F.T.; Hallikainen, M.T.; El-rayes, M.A. Microwave Dielectric Behavior of Wet Soil-Part II: Dielectric Mixing Models. *IEEE Trans. Geosci. Remote Sens.* **1985**, *GE-23*, 35–46. [CrossRef]

14. Ma, C.; Li, X.; Wang, S. A Global Sensitivity Analysis of Soil Parameters Associated With Backscattering Using the Advanced Integral Equation Model. *IEEE Trans. Geosci. Remote Sens.* **2015**, *53*, 5613–5623. [CrossRef]

15. Bindlish, R.; Barros, A.P. Parameterization of vegetation backscatter in radar-based, soil moisture estimation. *Remote Sens. Environ.* **2001**, *76*, 130–137. [CrossRef]

16. Ma, C.; Li, X.; Notarnicola, C.; Wang, S.; Wang, W. Uncertainty Quantification of Soil Moisture Estimations Based on a Bayesian Probabilistic Inversion. *IEEE Trans. Geosci. Remote Sens.* **2017**, *55*, 3194–3207. [CrossRef]

17. Oh, Y. Quantitative retrieval of soil moisture content and surface roughness from multipolarized radar observations of bare soil surfaces. *IEEE Trans. Geosci. Remote Sens.* **2004**, *42*, 596–601. [CrossRef]

18. Dubois, P.C.; Vanzyl, J.; Engman, T. Corrections to "Measuring Soil Moisture with Imaging Radars". *IEEE Trans. Geosci. Remote Sens.* **1995**, *33*, 1340. [CrossRef]

19. Fung, A.K.; Li, Z.Q.; Chen, K.S. Backscattering from a randomly rough dielectric surface. *IEEE Trans. Geosci. Remote Sens.* **1992**, *30*, 356–369. [CrossRef]

20. Chen, K.S.; Wu, T.D.; Tsang, L.; Qin, L.; Fung, A.K. Emission of rough surfaces calculated by the integral equation method with comparison to three-dimensional moment method simulations. *IEEE Trans. Geosci. Remote Sens.* **2003**, *41*, 90–101. [CrossRef]

21. Chen, K.S.; Wu, T.D.; Tsay, M.K.; Fung, A.K. Note on the multiple scattering in an IEM model. *IEEE Trans. Geosci. Remote Sens.* **2000**, *38*, 249–256. [CrossRef]

22. Baghdadi, N.; Saba, E.; Aubert, M.; Zribi, M.; Baup, F. Evaluation of Radar Backscattering Models IEM, Oh, and Dubois for SAR Data in X-Band Over Bare Soils. *IEEE Geosci. Remote Sens. Lett.* **2011**, *8*, 1160–1164. [CrossRef]

23. Ulaby, F.T.; Sarabandi, K.; Mcdonald, K.; Whitt, M.; Dobson, M.C. Michigan microwave canopy scattering model. *Int. J. Remote Sens.* **1990**, *11*, 1223–1253. [CrossRef]

24. Baghdadi, N.; El, H.M.; Zribi, M.; Bousbih, S. Calibration of the water cloud model at C-Band for winter crop fields and grasslands. *Remote Sens.* **2018**, *9*, 969. [CrossRef]

25. Merzouki, A.; Mcnairn, H.; Pacheco, A. Evaluation of the Dubois, Oh, and IEM radar backscatter models over agricultural fields using C-band RADARSAT-2 SAR image data. *Can. J. Remote Sens.* **2010**, *36*, S274–S286. [CrossRef]

26. Weiß, T.; Ramsauer, T.; Loew, A.; Marzahn, P. Evaluation of Different Radiative Transfer Models for Microwave Backscatter Estimation of Wheat Fields. *Remote Sens.* **2020**, *12*, 3037. [CrossRef]

27. Quan, X.; He, B.; Li, X. A Bayesian Network-Based Method to Alleviate the Ill-Posed Inverse Problem: A Case Study on Leaf Area Index and Canopy Water Content Retrieval. *IEEE Trans. Geosci. Remote Sens.* **2015**, *53*, 6507–6517. [CrossRef]

28. Kornelsen, K.C.; Coulibaly, P. Advances in soil moisture retrieval from synthetic aperture radar and hydrological applications. *J. Hydrol.* **2013**, *476*, 460–489. [CrossRef]

29. Hegarat-Mascle, S.L.; Zribi, M.; Alem, F.; Weisse, A.; Loumagne, C. Soil moisture estimation from ERS/SAR data: Toward an operational methodology. *IEEE Trans. Geosci. Remote Sens.* **2002**, *40*, 2647–2658. [CrossRef]

30. Joseph, A.T.; Van Der Velde, R.; O'Neill, P.E.; Lang, R.; Gish, T. Effects of corn on C- and L-band radar backscatter: A correction method for soil moisture retrieval. *Remote Sens. Environ.* **2010**, *114*, 2417–2430. [CrossRef]

31. van der Velde, R.; Su, Z.; Oevelen, P.V.; Wen, J.; Ma, Y.; Salama, M.S. Soil moisture mapping over the central part of the Tibetan Plateau using a series of ASAR WS images. *Remote Sens. Environ.* **2012**, *120*, 175–187. [CrossRef]

32. Quesney, A.; Hégarat-Mascle, S.L.; Taconet, O.; Vidal-Madjar, D.; Wigneron, J.P.; Loumagne, C.; Normand, M. Estimation of Watershed Soil Moisture Index from ERS/SAR Data. *Remote Sens. Environ.* **2000**, *72*, 290–303. [CrossRef]

33. Baghdadi, N.; Holah, N.; Zribi, M. Calibration of the Integral Equation Model for SAR data in C-band and HH and VV polarizations. *Int. J. Remote Sens.* **2006**, *27*, 805–816. [CrossRef]

34. De Roo, R.D.; Du, Y.; Ulaby, F.T.; Dobson, M.C. A semi-empirical backscattering model at L-band and C-band for a soybean canopy with soil moisture inversion. *IEEE Trans. Geosci. Remote Sens.* **2001**, *39*, 864–872. [CrossRef]

35. Bryant, R.; Moran, M.S.; Thoma, D.P.; Holifield Collins, C.D.; Skirvin, S.; Rahman, M.; Slocum, K.; Starks, P.; Bosch, D.; Gonzalez Dugo, M.P. Measuring Surface Roughness Height to Parameterize Radar Backscatter Models for Retrieval of Surface Soil Moisture. *IEEE Geosci. Remote Sens. Lett.* **2007**, *4*, 137–141. [CrossRef]

36. Merzouki, A.; Mcnairn, H.; Pacheco, A. Mapping Soil Moisture Using RADARSAT-2 Data and Local Autocorrelation Statistics. *IEEE J. Sel. Top. Appl. Earth Obs. Remote Sens.* **2011**, *4*, 128–137. [CrossRef]

37. Notarnicola, C.; Angiulli, M.; Posa, F. Soil Moisture Retrieval From Remotely Sensed Data: Neural Network Approach Versus Bayesian Method. *IEEE Trans. Geosci. Remote Sens.* **2008**, *46*, 547–557. [CrossRef]

38. Paloscia, S. A summary of experimental results to assess the contribution of SAR for mapping vegetation biomass and soil moisture. *Can. J. Remote Sens.* **2002**, *28*, 246–261. [CrossRef]

39. Zribi, M.; Hégarat-Mascle, S.L.; Ottlé, C.; Kammoun, B.; Guérin, C. Surface soil moisture estimation from the synergistic use of the (multi-incidence and multi-resolution) active microwave ERS Wind Scatterometer and SAR data. *Remote Sens. Environ.* **2003**, *86*, 30–41. [CrossRef]

40. Paloscia, S.; Pampaloni, P.; Pettinato, S.; Santi, E. A Comparison of Algorithms for Retrieving Soil Moisture from ENVISAT/ASAR Images. *IEEE Trans. Geosci. Remote Sens.* **2008**, *46*, 3274–3284. [CrossRef]

41. Zeng, J.; Li, Z.; Chen, Q.; Bi, H. Method for Soil Moisture and Surface Temperature Estimation in the Tibetan Plateau Using Spaceborne Radiometer Observations. *IEEE Geosci. Remote Sens. Lett.* **2015**, *12*, 97–101. [CrossRef]

42. Bai, X.; He, B.; Li, X.; Zeng, J.; Wang, X.; Wang, Z.; Zeng, Y.; Su, Z. First Assessment of Sentinel-1A Data for Surface Soil Moisture Estimations Using a Coupled Water Cloud Model and Advanced Integral Equation Model over the Tibetan Plateau. *Remote Sens.* **2017**, *9*, 714. [CrossRef]

43. Attema, E.; Ulaby, F. Vegetation modeled as a water cloud. *Radio Sci.* **1978**, *13*, 357–364. [CrossRef]

44. Jackson, T.J.; Le Vine, D.M.; Hsu, A.Y.; Oldak, A.; Starks, P.J.; Swift, C.T.; Isham, J.D.; Haken, M. Soil moisture mapping at regional scales using microwave radiometry: The Southern Great Plains Hydrology Experiment. *IEEE Trans. Geosci. Remote Sens.* **1999**, *37*, 2136–2151. [CrossRef]

45. Zhao, L.; Yang, K.; Qin, J.; Chen, Y.; Tang, W.; Lu, H.; Yang, Z. The scale-dependence of SMOS soil moisture accuracy and its improvement through land data assimilation in the central Tibetan Plateau. *Remote Sens. Environ.* **2014**, *152*, 345–355. [CrossRef]

46. Van der Velde, R.; Su, Z.; Ma, Y. Impact of Soil Moisture Dynamics on ASAR σo Signatures and Its Spatial Variability Observed over the Tibetan Plateau. *Sensors* **2008**, *8*, 5479–5491. [CrossRef]

47. Ren, Y.; Yang, K.; Wang, H.; Zhao, L.; Chen, Y.; Zhou, X.; La, Z. The South Asia Monsoon Break Promotes Grass Growth on the Tibetan Plateau. *J. Geophys. Res. Biogeosci.* **2021**, *126*. [CrossRef]

48. Lu, H.; Wang, W.; Tian, F.; Yang, K. Improving satellite rainfall estimates over Tibetan plateau using in situ soil moisture observation and SMAP retrievals. In Proceedings of the International Geoscience and Remote Sensing Symposium, Fort Worth, TX, USA, 23–28 July 2017; pp. 2004–2007.

49. Yang, K.; Qin, J.; Zhao, L.; Chen, Y.; Tang, W.; Han, M.; Zhu, L.; Chen, Z.; Lv, N.; Ding, B.; et al. A Multiscale Soil Moisture and Freeze-Thaw Monitoring Network on the Third Pole. *Bull. Am. Meteorol. Soc.* **2013**, *94*, 1907–1916. [CrossRef]

50. Amazirh, A.; Merlin, O.; Er-Raki, S.; Gao, Q.; Rivalland, V.; Malbeteau, Y.; Khabba, S.; Escorihuela, M.J. Retrieving surface soil moisture at high spatio-temporal resolution from a synergy between Sentinel-1 radar and Landsat thermal data: A study case over bare soil. *Remote Sens. Environ.* **2018**, *211*, 321–337. [CrossRef]

51. Bousbih, S.; Zribi, M.; Lili-Chabaane, Z.; Baghdadi, N.; Hajj, M.E.; Gao, Q.; Mougenot, B. Potential of Sentinel-1 Radar Data for the Assessment of Soil and Cereal Cover Parameters. *Sensors* **2017**, *17*, 2617. [CrossRef]

52. Didan, K.; Munoz, A.B.; Solano, R.; Huete, A. *MODIS Vegetation Index User's Guide (MOD13 Series)*; Vegetation Index and Phenology Lab, University of Arizona: Tucson, AZ, USA, 2015.

53. Wang, H.; Ramata, M.; Kalifa, G. Potential of a two-component polarimetric decomposition at C-band for soil moisture retrieval over agricultural fields. *Remote Sens. Environ.* **2018**, *217*, 38–51. [CrossRef]

54. Gherboudj, I.; Magagi, R.; Berg, A.A.; Toth, B. Soil moisture retrieval over agricultural fields from multi-polarized and multi-angular RADARSAT-2 SAR data. *Remote Sens. Environ.* **2011**, *115*, 33–43. [CrossRef]

55. Zribi, M.; Gorrab, A.; Baghdadi, N. A newsoil roughness parameter for themodelling of radar backscattering over bare soil. *Remote Sens. Environ.* **2014**, *152*, 62–73. [CrossRef]

56. Chan, S.; Bindlish, R.; Hunt, R.; Jackson, T.J.; Kimball, J. *Soil Moisture Active Passive (SMAP) Ancillary Data Report: Vegetation Water Content*; Jet Propulsion Laboratory: Pasadena, CA, USA, 2013.

57. Wang, H.; Magagi, R.; Goita, K.; Wang, K. Soil moisture retrievals using ALOS2-ScanSAR and MODIS synergy over Tibetan Plateau. *Remote Sens. Environ.* **2020**, *251*, 112100. [CrossRef]

58. Srivastava, H.S.; Patel, P.; Manchanda, M.L.; Adiga, S. Use of multiincidence angle RADARSAT-1 SAR data to incorporate the effect of surface roughness in soil moisture estimation. *IEEE Trans. Geosci. Remote Sens.* **2003**, *41*, 1638–1640. [CrossRef]

59. Ma, C.; Li, X.; Mccabe, M.F. Retrieval of High-Resolution Soil Moisture through Combination of Sentinel-1 and Sentinel-2 Data. *Remote Sens.* **2020**, *12*, 2303. [CrossRef]

60. van der Velde, R.; Su, Z.; Wen, J. Roughness determination from multi-angular ASAR Wide Swath mode observations for soil moisture retrieval over the Tibetan Plateau. In Proceedings of the Eusar European Conference on Synthetic Aperture Radar, Berlin, Germany, 3–5 June 2014.

61. Chai, X.; Zhang, T.; Shao, Y.; Gong, H.; Liu, L.; Xie, K. Modeling and Mapping Soil Moisture of Plateau Pasture Using RADARSAT-2 Imagery. *Remote Sens.* **2015**, *7*, 1279–1299. [CrossRef]

62. Baghdadi, N.; Zribi, M.; Loumagne, C.; Ansart, P.; Anguela, T.P. Analysis of TerraSAR-X data and their sensitivity to soil surface parameters over bare agricultural fields. *Remote Sens. Environ.* **2008**, *112*, 4370–4379. [CrossRef]

63. Baghdadi, N.; King, C.; Chanzy, A.; Wigneron, J.P. An empirical calibration of the integral equation model based on SAR data, soil moisture and surface roughness measurement over bare soils. *Int. J. Remote Sens.* **2002**, *23*, 4325–4340. [CrossRef]

64. Callens, M.; Verhoest, N.E.C.; Davidson, M.W.J. Parameterization of tillage-induced single-scale soil roughness from 4-m profiles. *IEEE Trans. Geosci. Remote Sens.* **2006**, *44*, 878–888. [CrossRef]
65. Wagner, W.; Blöschl, G.; Pampaloni, P.; Calvet, J.C.; Bizzarri, B.; Wigneron, J.P.; Kerr, Y. Operational readiness of microwave remote sensing of soil moisture for hydrologic applications. *Hydrol. Res.* **2007**, *38*, 1–20. [CrossRef]
66. Verhoest, N.E.C.; Lievens, H.; Wagner, W.; Álvarez-Mozos, J.; Moran, M.S.; Mattia, F. On the Soil Roughness Parameterization Problem in Soil Moisture Retrieval of Bare Surfaces from Synthetic Aperture Radar. *Sensors* **2008**, *8*, 4213–4248. [CrossRef]
67. Bai, X.; He, B.; Li, X. Optimum Surface Roughness to Parameterize Advanced Integral Equation Model for Soil Moisture Retrieval in Prairie Area Using Radarsat-2 Data. *IEEE Trans. Geosci. Remote Sens.* **2016**, *54*, 1–12. [CrossRef]
68. Peischl, S.; Walker, J.P.; Ryu, D.; Kerr, Y.H.; Panciera, R.; Rudiger, C. Wheat Canopy Structure and Surface Roughness Effects on Multiangle Observations at L-Band. *IEEE Trans. Geosci. Remote Sens.* **2012**, *50*, 1498–1506. [CrossRef]